ANALYTICAL SIMULATION OF

WELD EFFECTS IN CREEP RANGE

A.K. Dhalla
Westinghouse Electric Corporation
Advanced Energy Systems Division
Madison, Pennsylvania 15663

The purpose of this paper is to present the inelastic analysis procedure used to investigate the effect of welding on the creep rupture strength of a typical Liquid Metal Fast Breeder Reactor (LMFBR) nozzle. The current study is part of an overall experimental and analytical investigation to verify the inelastic analysis procedure now being used to design LMFBR structural components operating at elevated temperatures. Two important weld effects included in the numerical analysis are: (a) the residual stress introduced in the fabrication process, and (b) the time-independent and the time-dependent material property variations. Finite element inelastic analysis was performed on a CRAY-1S computer using the ABAQUS program with the constitutive equations developed for the design of LMFBR structural components. The predicted peak weld residual stresses relax by as much as 40% during elevated temperature operation, and their effect on creep-rupture cracking of the nozzle is considered of secondary importance.

INTRODUCTION

A test facility was designed and built to perform thermal transient load tests on prototypic Liquid Metal Fast Breeder (LMFBR) Intermediate Heat Exchanger (IHX) inlet and outlet nozzles. Three prototypic nozzles forged from type 304 stainless steel were welded equidistantly around the circumference of the cylinder as shown in Figure 1.

All nozzles were subjected to internal pressure (p) and creep hold time (t) in a two stage creep-ratcheting test at a temperature of 1100°F (593°C): (a) Stage 1--p = 200 psi (1.4 MPa) and t = 1400 hours, and (b) Stage 2--p = 450 psi (3.1 MPa) and t = 3000 hours. One of the shell nozzles was subjected to a total of 26 thermal downshock transients; the remaining nozzles in the test article were baffled off and did not experience thermal transients. After each transient the pressure vessel was depressurized, repressurized, and uniformly heated and held at a temperature of 1100°F (593°C) for about 160 hours of creep hold time before initiating the next thermal transient. Post-test liquid dye penetrant examination revealed cracks parallel and perpendicular to the weld in the heat affected zone (HAZ) on nozzle side of all the shell nozzles. A metallurgical examination revealed that creep-rupture was the major cause of these cracks.

The investigation reported here is part of an overall experimental and analytical investigation to verify inelastic analysis procedures used to predict the creep ratcheting and the creep-rupture failure in welded structural components operating at elevated temperature. This paper presents only the analytical procedure used to investigate the weld residual stress relaxation and weld material property variation in a prototypic LMFBR-IHX shell nozzle. The following three specific areas are discussed:

1. selection of an appropriate 3-D mesh in the weld region.

2. representation of time-independent and time-dependent material response based upon uniaxial tensile and creep test data.

3. simulation of weld shrinkage due to weld cool-down.

The predicted peak effective, circumferential and longitudinal weld residual stresses relax by about 40% during elevated temperature operation, and their effect on cracking is considered of secondary importance. In subsequent discussion, the maximum weld residual stress parallel to the weld slice around the nozzle – cylinder intersection is designated as a circumferential stress, and the intermediate principal stress along the nozzle and perpendicular to the weld slice is designated as a longitudinal stress.

FINITE ELEMENT IDEALIZATION OF THE SHELL NOZZLE GEOMETRY

Three planes of symmetry were advantageously utilized to generate the refined finite element mesh shown in Figure 2 which represents the as-built nozzle geometry. The as-built nozzle sections were measured by the fabricator (Foster Wheeler Energy Applications, Inc.) after final machining but before the nozzles were welded to the cylindrical shell. The geometric dimensions of the as-built cross-sections of the nozzle were transferred via a Digitizing Tablet linked to the FIGURES-II interactive mesh generation program [1].* The finite element analysis was performed on a CRAY-1S computer using Version-4 of the ABAQUS computer program [2]. A reduced integration (2x2x2) scheme was used to obtain better accuracy at integration points than that predicted by the full (3x3x3) integration scheme [3]. The reduced integration option of the ABAQUS program uses a higher order (3x3x3) integration to form element stiffnesses and the distributed loads are integrated fully, but stresses and strains are calculated only at the reduced (2x2x2) integration points. To utilize computer resources more efficiently and to improve overall accuracy of predictions, it is preferable to use more elements in the nozzle weld region with reduced integration instead of using more integration points per element.

Boundary Conditions

In addition to the symmetric boundary conditions along the transverse, longitudinal and 60° symmetry planes shown in Figure 2, it was necessary to apply appropriate end cap pressure loadings and displacement boundary conditions to the finite element model. The pipe welded to the nozzle is

*Numerals in brackets designate references at the end of this paper.

quite flexible, hence the end cap pressure loading was applied to the pipe attachment of the nozzle without restraining the ovalization deformations of the nozzle end. In contrast, two hemispherical heads welded to the cylinder constrain free ovalization deformations of the cylinder ends. This effect was included in the analysis by constraining the circular cylinder end section to expand only axisymmetrically; end cap pressure was also applied to the cylinder end.

Convergence Study

Three elastic analyses were performed to evaluate the convergence characteristics of the 20-node isoparametric (tri-quadratic) element of the ABAQUS computer program. To select an economical mesh in the weld region internal pressure was applied to the nozzle. The three finite element models evaluated in this study are designated as:

1. I-Q1: Coarse surface mesh (72 elements), and one tri-quadratic continuum element through the thickness.

2. A-Q1: Refined surface mesh (108 elements) near the weld region, and one tri-quadratic element through the thickness.

3. A-Q3: Refined surface mesh (108 elements) near the weld region, and three tri-quadratic elements through the thickness.

The effect of weld region surface mesh refinement is shown in Figure 3. The component stress distributions predicted from the I-Q1 and A-Q1 models are in good agreement except near the weld. The surface mesh model I-Q1 is coarse and any as-built thickness variations are smoothed out. In contrast, the solid line stress distributions predicted by the A-Q1 analysis show significant irregular variation of stresses due to as-built thickness variations in the vicinity of the weld. The insert in Figure 3 shows the irregular thickness variation and slope discontinuity at the transverse section near the weld. The maximum change in thickness is from 1.19 to 1.29 inches (about 8%). The stress variations predicted by model A-Q1 near the weld are not directly proportional to the thickness because the stress distribution near the nozzle cylinder intersection is not uniform through the thickness and around the doubly curved nozzle surface.

The effects of mesh refinement through the thickness are illustrated in Figure 4, where the σ_x and σ_y stress components are plotted at the highly stressed welded location on the transverse section. The stress distributions predicted by the one and three element models (A-Q1 and A-Q3) with the same surface mesh of 108 elements are in good agreement. Similar good agreement was observed at other locations in the nozzle. Either of these two models would have been adequate for final analysis; however, the three element refined model (A-Q3) was selected for final inelastic analysis to include stress distributions through the thickness that would occur due to temperature variations during the simulated weld cool-down process.

MATERIAL MODEL FOR INELASTIC ANALYSIS

A spare nozzle forging of the same heat of material was sectioned to obtain tensile and creep material property data in circumferential and longitudinal directions from various locations in the nozzle forging. Thirteen short term tensile tests and six short term cyclic tests were performed on specimens extracted from the spare nozzle at temperatures ranging from 70 to 1100°F (21 to 593°C) to obtain time-independent stress-strain curves for elastic-plastic analysis. Twenty-two creep tests and nine relaxation tests were performed at two temperatures, 1050 and 1100°F (566 and 593°C), to obtain time-dependent creep properties. Four tensile and eight creep tests were also performed on uniaxial miniature specimens fabricated from the HAZ and the weld material. The test specimens were along the nozzle (longitudinal) and perpendicular to the circumferential weld slice.

The creep and tensile material test data indicate that properties change rapidly within a distance of 1 inch (25 mm) of the weld region of the nozzle-cylinder intersection. Although the change is continuous, from weld to HAZ to the nozzle forging base metal, in the finite element idealization it was necessary to simulate this change as a stepwise function. To simulate the observed material property variation at a reasonable computation cost, a five zone material model was developed for the nozzle side of the nozzle-cylinder intersection, where creep-rupture cracks were observed in the experiment. The creep-rupture cracks, as well as slip traces, were observed as far away as 0.5 in. (12 mm) from the weld. Material model presented in this paper reflects the nozzle material work hardening and other material property changes due to welding.

Time-Independent Material Model

The time-independent isothermal tension coupon tests conducted on the nozzle forging material at 1100°F (593°C) show a significant scatter in Figure 5. This figure displays both monotonic (first cycle) and tenth cycle test data, along with the ASME Code curves for type 304 stainless steel material. The base metal data are within the scatterband represented by the ASME minimum and average curves shown as solid lines. The curve designated as BASE METAL represents a reasonable average of specimens extracted from different locations in the nozzle forging. The nozzle weldment test results are designated as WELD and HAZ in Figure 5. To comply with the constitutive theory of linear kinematic hardening, it was necessary to bilinearize the stress strain curves obtained from the weld, HAZ and base metal of the nozzle. Figure 6 shows the decrease in bilinear yield stress with respect to the distance from the weld.

Temperature in the weld region during weld cool-down varies from room temperature to 2000°F (1093°C). Therefore, to predict residual stresses it is necessary to include temperature dependence of material properties in the analysis. The tests performed on the nozzle material were not sufficient to develop a complete temperature dependent material model. Therefore,

engineering judgment was used to utilize and extrapolate the data available in the ASME Code. The material property variations presented in [4 to 6] also provided guidance in the selection of the material model.

Temperature dependence of yield stress σ_y and plastic slope ($E_p = \Delta\sigma/\Delta\varepsilon_p$) are shown in Figures 7 and 8, respectively. The idealized variations to be used in analysis are shown as dotted lines. A finite, but small, value was assumed for both σ_y and E_p at 2000°F (1093°C). At that temperature the material is liquidus and cannot sustain significant stress. For weld and the HAZs, the variations with respect to temperature were assumed to be the same as those for the base metal up to 1500°F (816°C); thereafter, the corresponding values at 1500°F (816°C) were linearly connected to the finite value of 1 ksi (6.9 MPa) at 2000°F (1093°C). The temperature dependent material property variations of Young's Modulus E, Poisson Ratio, ν, and coefficient of thermal expansion, α are given in Table 1.

TABLE 1.-TEMPERATURE DEPENDENT MATERIAL PROPERTIES FOR TYPE 304 STAINLESS STEEL

MODULUS OF ELASTICITY (E)

$$E\ (ksi) = [28.31 \times 10^3 - 5.286\ (T-70)]\quad 70 < T < 700$$
$$= [24.98 \times 10^3 - 8.16\ (T-700)]\quad 700 < T < 1200$$
$$= [20.9 \times 10^3 - 24.88\ (T-1200)]\quad 1200 < T < 2000$$

POISSON'S RATIO (ν)

$$\nu = [0.2672 - 4.02 \times 10^{-5}\ (T-70)]\quad 70 < T < 2000$$

COEFFICIENT OF THERMAL EXPANSION (α)

$$\alpha\ (/°F) = [8.58 \times 10^{-6} + 1.82 \times 10^{-9}\ (T-70)]\quad 70 < T < 700$$
$$= [9.73 \times 10^{-6} + 1.13 \times 10^{-9}\ (T-700)]\quad 700 < T < 2000$$

Note: Temperature T is in degrees Fahrenheit.

Time-Dependent Creep Model

Twenty-two uniaxial constant load creep tests on specimens fabricated from the spare nozzle forging were conducted at stress levels ranging from 7.5 to 25 ksi (51.7 to 172.4 MPa). Eight additional creep and/or creep-rupture tests were also performed to obtain data for the HAZ and the weld region of the nozzle. Initially, attention was focused on developing an appropriate analytical representation from creep data obtained for the base metal. Thereafter, the analytical representation was extended to simulate the weld and HAZ creep data.

The experimental base metal data are compared in Figures 9a and 9b with available creep curves for type 304 stainless steel material. Typical comparisons are shown at only two stress levels: a low stress of 10 ksi (68.9 MPa) and a high stress of 20 ksi (137.9 MPa). The numerals 1 and 2 designate the single exponential (1-Exp.) and the double exponential (2-Exp.) creep equations developed for specific heats of type 304 SS material. The letters A and O designate the "ORNL ALL DATA" and "1000 HOUR DATA" creep equations developed by Oak Ridge National Laboratory for a specific heat of type 304 SS material. The letter C designates the nozzle forging base metal creep data and the letter R designates the final best-fit rational polynomial creep equation used in this study. A comparison of uniaxial creep data and the available mathematical representations show that the correlation between measured data and the analytical curve 'R' developed for the present study is quite good.

The rational polynomial creep equation form selected for the present study is as follows:

$$\varepsilon_c = \frac{Cpt}{(1 + pt)} + \dot{\varepsilon}_m t \qquad (1)$$

where, ε_c is the total creep strain in %; C is the amount of transient creep strain in %; p is the primary creep parameter in 1/hr, which relates to sharpness of curvature of primary creep region; $\dot{\varepsilon}_m$ is the minimum creep rate in %/hr; and t is the elapsed time in hr. Booker, et al., [7] have developed functional relationships for C and p in terms of $\dot{\varepsilon}_m$, with $\dot{\varepsilon}_m$ having a term C_h' (lot constant) to adjust for differences between heats of the material.

The minimum creep rate, in Equation (1), is a known quantity that is obtained from each uniaxial creep test. Based upon $\dot{\varepsilon}_m$ and the average lot constant, C_h', the primary creep parameters C and p were calculated according to the relationships presented in [7]. The creep strains predicted by the rational polynomial creep equation (1) are compared with the experimental data in Figures 10a and 10b for the low and high stress levels. The measured creep strains (designated by a letter C) are not in good agreement with the rational polynomial predictions (designated by numeral 1), which were calculated according to the procedure presented in [7]. Consequently, it was necessary to adjust constants C and p in Equation (1) to obtain a better fit to the creep data, especially to the initial primary creep strain rates, which in the analysis would determine the relaxation of residual stress due to weld effects. Various combinations of constants C and p were examined. A

reasonable fit to creep data (designated by numeral 3 in Figures 10a and 10b) was obtained by adjusting the constants C and p. That is, to obtain curve 3 from curve 1, the constant C calculated as per [7] was reduced by a factor of 3 and the constant p was increased by a factor of 9. The adjusted rational polynomial creep equation (designated as curve 3 in these figures) is adequate to represent creep response of the nozzle forging material.

The uniaxial data obtained from the HAZ and the weld material indicate that the weld region is substantially stronger (lower creep rates) than the base metal. To develop a material model for the weld region, the creep equation constants C and p were appropriately adjusted to obtain reasonably smooth variations of creep rates between the weld and the nozzle forging. The rational polynomial creep curves for five zones in the weld region are shown in Figure 11. The nozzle forging and the weld metal analytical curves are designated by numerals 1 and 5, respectively.

The rational polynomial creep model developed here is considered adequate to simulate the creep response in the nozzle analysis, however, the actual properties used in the analytical model are difficult to justify in all respects because:

1. the extent of heat affected zone (HAZ) in the as-built nozzle cannot be defined accurately,

2. the size and the number of finite elements used in the analytical model to represent the weld region require discontinuous representation of the material properties, and

3. the scatter in uniaxial material data [8] requires some approximation in the analytical representation.

THERMAL LOADING TO SIMULATE RESIDUAL STRESSES DURING WELD COOL-DOWN PROCESS

The distribution and the peak amplitude of the residual stress introduced during the welding process depend upon many variables. A few of these variables mentioned in the literature [9 to 12] are: (a) plate thickness, (b) heat input, (c) rate of cooling (heat sink, surface convection and radiation, etc., in complex geometries), (d) shift in peak temperatures during the cooling process, (e) weld repair (if any), (f) geometric configuration of the weld groove, (g) number of weld passes, and (h) geometry and size of the welded component.

Temperature Profiles Developed for the Nozzle

The purpose of the present investigation is to evaluate the relaxation and subsequent redistribution of residual stresses during creep hold time of 1100°F (593°C). Consequently, it is not necessary to simulate accurately the residual stress distribution, and predict the peak residual stress in the nozzle. An overall simulation of residual stress distribution was

accomplished by specifying temperature distributions due to the last weld pass cool-down on the outside surface. Typical weld thermal cycle charts presented in the Welding Handbook [9] show that:

1. the cooling rate of a weld and the width of the corresponding HAZ can be controlled by manipulating energy input and preheat temperature,

2. the cooling rate increases with increase in plate thickness,

3. the time at elevated-temperature decreases with increase in plate thickness, and

4. the heat flow pattern changes from a two-dimensional flow for very thin plates to a three-dimensional flow for very thick plates. The heat flow change qualitatively explains the influence of plate thickness on cooling rates.

Figure 12, taken from [10], shows the weld cool-down rate measured with respect to time and distance for a 1.3 in. (33 mm) thick 26 in. (660 mm) diameter type 304 stainless steel butt welded pipe. The weld and geometric parameters for the welded pipe, although similar, are not the same as those used to fabricate the nozzle test assembly. Temperature profiles during weld cool-down were not measured in the nozzle experiment, therefore, the temperature distributions shown in Figure 12 were used to generate temperature profiles for the nozzle weld cool-down analysis. Time dependent temperature profiles along the nozzle are shown in Figures 13a to 13c for three layers (outside, middle, and inside) through the thickness of the weld region. These nodal temperature distributions along the nozzle are assumed to be circumferentially symmetric (axisymmetric with respect to the nozzle centerline).

Figures 13a and 13c show that the temperature decreases rapidly away from the weld and within 50 seconds the highest temperature of 800°F (427°C) is below the creep range of type 304 stainless steel. Also the temperature decreases below 800°F at a distance of about 0.5 inch (13 mm) away from the edge of the weld. The analytical simulation of the nozzle weld cool-down process shown in Figures 13a to 13c is consistent with the temperature measurements presented in [9 and 10]. The metal temperatures up to a distance of about 0.8 in. (20.3 mm) from the welded hot spot decrease with elapsed time, whereas the metal temperatures at distances greater than 0.8 in. (20.3 mm) increase with elapsed time, up to about 50 seconds, before reaching a steady state uniform temperature distribution of 200°F (93°C). To further simplify the analysis, the weld deposition (heat-up) process was not simulated. The justification is that at the end of heat-up the weld would be liquidus at temperatures above 2000°F (1093°C), and would not be able to sustain significant stresses before it cools down.

Loading History for Weld Residual Stress Analysis

The following steps summarize the loading history used to perform the inelastic analysis:

1. Assume an initial stress-free state at a time less than 3 seconds for temperature distribution shown in Figures 13a to 13c, with 200°F (93°C) uniform temperature away from the weld.

2. Apply temperature distributions at times of 20 sec., 50 sec., and greater than 2000 secs. to simulate the weld cool-down process.

3. Heat-up to 1100°F (593°C) uniform operating temperature, hold at elevated temperature (without pressure) for 156 hours and cool-down to 70°F (21°C) ambient temperature.

INELASTIC ANALYSIS RESULTS

The inelastic analysis was performed in accordance with the constitutive equations recommended in [13] for the LMFBR structural components operating at elevated temperature. Figures 14a to 14c show deformations of the nozzle at the end of 156 hours of creep hold time. These deformations include free thermal deformations of the nozzle. The dotted lines in these figures represent the original nozzle geometry and the solid lines show the deformed shape, where the displacements are magnified 100 times. Figure 14a shows the overall deformations, whereas Figures 14b and 14c show two deformed sections along the length of the nozzle: (a) longitudinal section and (b) transverse section. The weld shrinkage effects are clearly seen in these figures. At distances away from the weld, free thermal expansion deformation is large but the differential thermal deformation between contiguous elements is small. Consequently, the residual stresses away from the weld region are small. Thus the stress distribution of interest is around the weld slice--a circumferential set of elements around the nozzle-cylinder intersection.

Figure 15 shows distribution of two principal stresses (circumferential and longitudinal) around the nozzle weld slice. The maximum principal residual stress is in the circumferential direction. Two curves for each principal stress in this figure show that the residual stresses decrease when the test article is uniformly heated from 200°F (93°C--cold state) to an operating temperature of 1100°F (593°C--hot state). At 200°F (93°C) the residual stresses are on the yield surface; at the 1100°F (593°C) operating temperature the yield surface shrinks and residual stresses decrease to satisfy the flow rule of the material.

Residual Stress Distribution

Figures 16 and 17 show the circumferential stress and effective plastic strain distributions along the longitudinal and transverse sections. The stress and strain predictions are plotted at the boundary of two contiguous finite elements as an average of two integration points to present smoothed stress distribution in these figures. The distributions are displayed along the inside surface of the longitudinal section in Figure 16, and along the outside surface of the transverse section in Figure 17.

The stress and strain profiles along the length of the nozzle, shown in Figures 16 and 17, indicate that the peak stress levels are predicted near the weld as anticipated. At the end of creep hold time of 156 hours the peak residual stresses near the weld region relax by as much as 40%. Longitudinal and effective peak stresses also relaxed by about the same amount. The maximum plastic strain of about 1.4% is accumulated at the transverse section of the weld slice (Figure 17). The residual stress relaxation predicted here is consistent with relaxation results presented in [14 and 15] for circumferentially welded pipes.

After completing the weld cool-down analysis, the nozzle was subjected to the internal pressure loadings and creep hold times recorded in the experiment. The creep-rupture predictions, which will be presented in a separate paper [16], indicate that the observed creep-rupture cracking parallel to weld is not due to the presence of weld residual stresses. The maximum principal residual stress is parallel and not perpendicular to the observed circumferential cracking on the outside surface. The secondary importance of residual stress on cracking can also be judged by the fact that the weld residual stresses relax rapidly during creep hold time. In contrast, the internal pressure stresses do not relax significantly and the maximum principal pressure stress is aligned perpendicular to the observed cracking. Therefore, the primary cause of cracking observed in the experiment is due to the pressure stresses [16].

CONCLUDING REMARKS

A 3-D finite element model consisting of 324 tri-quadratic elements of the ABAQUS computer program was used to predict residual stresses in a prototypic LMFBR nozzle. The weld shrinkage effects and the residual stresses were simulated numerically by specifying time-dependent temperature profiles for the nozzle weld. The variation of time-independent and time-dependent analytical material models for the weld region were established from the uniaxial tensile and creep tests of the nozzle weldment material.

The deformation plots of the nozzle after weld cool-down qualitatively show that the analysis simulated the weld shrinkage effects very well. Two highly stressed regions where cracks were observed in the experiment were correctly identified by the analysis. The maximum residual stresses occur on either side of the weld, and attenuate away from the weld region. In the absence of experimental measurements, the residual stress distributions predicted by the inelastic nozzle weld analysis are considered reasonable, especially at highly stressed nozzle locations where the residual stresses are limited by the yield surface specified for the weld, HAZ and nozzle forging material. An important conclusion from this analytical study is that the peak residual stresses relax by as much as 40% during elevated-temperature operation.

The present study is part of an overall analytical investigation undertaken to evaluate the effect of weld residual stresses on creep-rupture failure of structural components operating in creep range. In a separate

paper [16] it is shown that the residual stresses raise the total stresses predicted in the internally pressurized nozzle; however, the observed circumferential cracking (parallel to weld) on the outside surface of the nozzle is parallel to the maximum principal residual stress.

A detailed evaluation of analytical predictions in [16] show that the effect of residual stresses on creep-rupture cracking is of secondary importance. The primary reasons for nozzle weld cracking are: (a) the principal pressure stresses which are perpendicular to the observed cracks and do not relax significantly during creep hold time, and (b) the weld effect in the form of higher HAZ and weld material yield strength with about the same or slightly lower creep-rupture strength than that of the base metal.

ACKNOWLEDGEMENTS

This paper is based upon work performed for the U.S. Department of Energy under Contract DE-AM02-76CH94000. The author expresses his appreciation to Dr. D. S. Griffin for his valuable comments during the course of this investigation.

REFERENCES

[1] FIGURES II User's Guide, Westinghouse R&D Center, Pittsburgh, PA, 1983.

[2] ABAQUS User's Manuals, Vols. 1-4, Hibbitt, Karlsson and Sorensen, Inc., Providence, RI, 1982.

[3] J. Barlow, "Optimal Stress Locations in Finite Element Models," Int. J. Num. Meth. Engng., 10, pp. 243-251 (1976).

[4] E. F. Rybicki, D. W. Schmueser, R. W. Stonesifer, et al., "A Finite-Element Model for Residual Stresses and Deflections in Girth-Butt Welded Pipes," Trans. ASME, J. Press. Vessel Tech., 100, pp. 256-262 (1978).

[5] M. J. Davidson, C. W. Lawton and R. W. Loomis, "Bimetallic Weld Residual Stress Field," in Properties of Steel Weldments for Elevated Temperature Pressure Containment Applications, MPC-9, pp. 175-182, American Society of Mechanical Engineers, New York, NY, 1978.

[6] Y. Ueda, K. Fukuda, and K. Nakacho, et al. "Basic Procedures in Analysis and Measurement of Welding Residual Stresses by the Finite Element Method," in Residual Stresses in Welded Construction and their Effects, pp. 27-37, The Welding Institute, London, England, 1977.

[7] M. K. Booker and B. L. P. Booker, "New Methods for Analysis of Material Strength Data for the ASME B&PV Code," in Use of Computers in Managing Material Property Data, MPC-14, pp. 31-64, American Society of Mechanical Engineers, New York, NY, 1980.

[8] V. K. Sikka, M. K. Booker, and C. R. Brinkman, "Relationship Between Short- and Long-term Mechanical Properties of Several Austenitic Stainless Steels," in Characterization of Materials for Service at Elevated Temperatures, MPC-7, pp. 51-82, American Society of Mechanical Engineers, New York, NY, 1978.

[9] C. M. Adams, Jr., "Heat Flow in Welding," in Welding Handbook, Vol. 1, Ch. 3, 7th Ed., pp. 80-98, American Welding Society, Miami, FL, 1976.

[10] F. W. Brust and R. B. Stonesifer, "Effect of Weld Parameters on Residual Stresses in BWR Piping Systems, Final Report, " EPRI-NP-1743, March 1981.

[11] W. J. Shack, W. A. Ellingson, and L. E. Pahis, "Measurement of Residual Stresses in Type-304 Stainless Steel Piping Butt Weldments, Phase Report," EPRI-NP-1413, June 1980.

[12] A. J. Giannuzzi, D. C. Bertossa, P. P. Hallila, et al., "Studies on AISI Type 304 Stainless Steels Piping Weldments for Use in BWR Application Fifth Quarterly Progress Report for April, May, June 1976," NEDO-20985-5, August 1976.

[13] C. E. Pugh and D. N. Robinson, "Some Trends in Constitutive Equation Model Development for High-Temperature Behavior of Fast-Reactor Structural Alloys," Nucl. Eng. and Des. 48, pp. 269-276 (1978).

[14] R. Fidler, "The Effect of Time and Temperature on Residual Stresses in Austenitic Welds," Trans. ASME, J. Press. Vessel Tech, 104, pp. 210-214 (1982).

[15] S. Nair, E. Pang, and R. C. Dix, "Residual Stress Generation and Relaxation in Butt-Welded Pipes," Trans. ASME, J. Press. Vessel Tech., 104, pp. 42-46 (1982).

[16] A. K. Dhalla, "Effect of Residual Stress on Creep-Rupture Strength of a Prototypic Welded Nozzle," (in preparation).

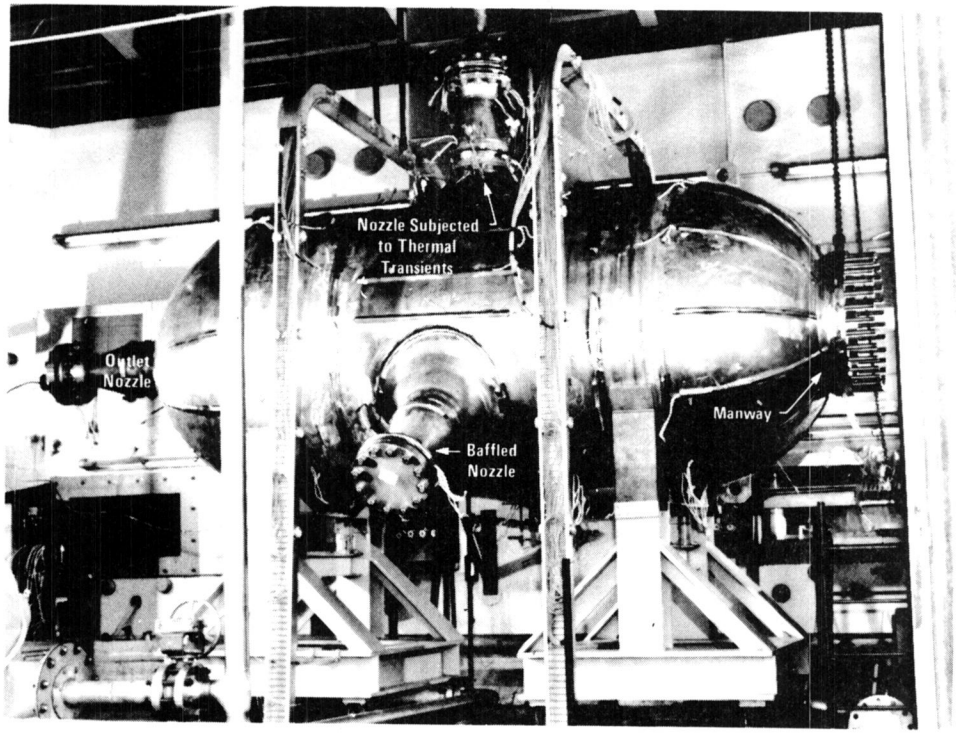

Figure 1. - Full Scale Pressure Vessel Nozzles were tested and analyzed to validate methods of analysis and design criteria

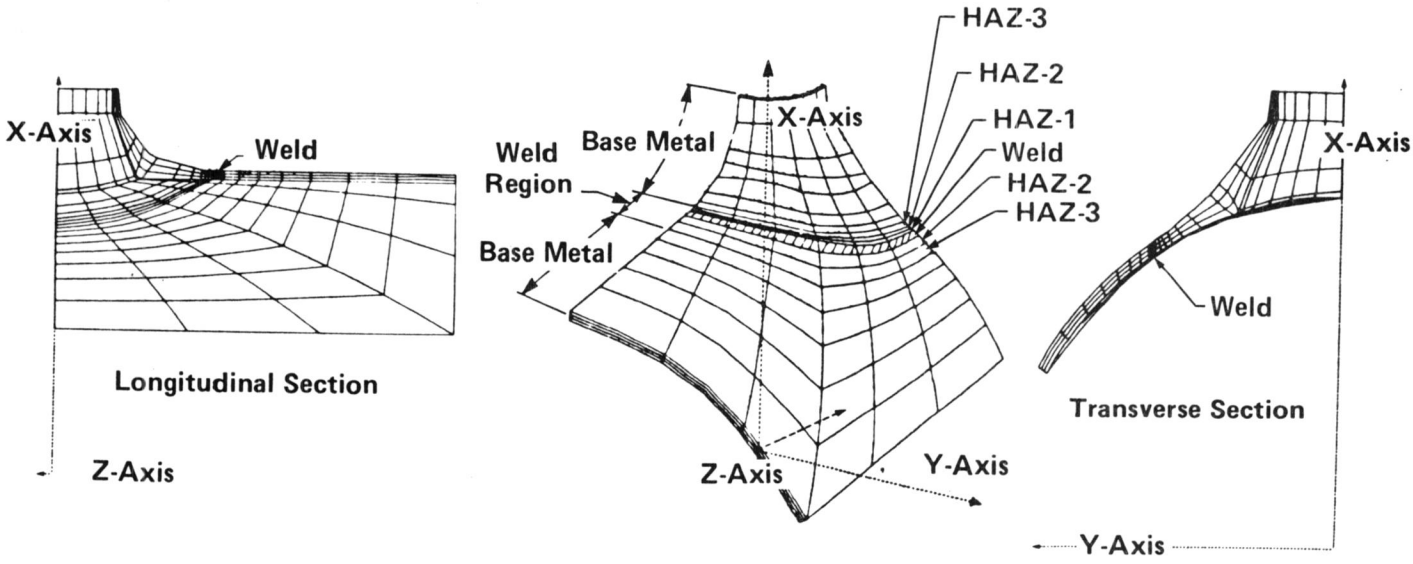

Figure 2. - Finite Element Idealization of As-Built Inlet Nozzle Geometry

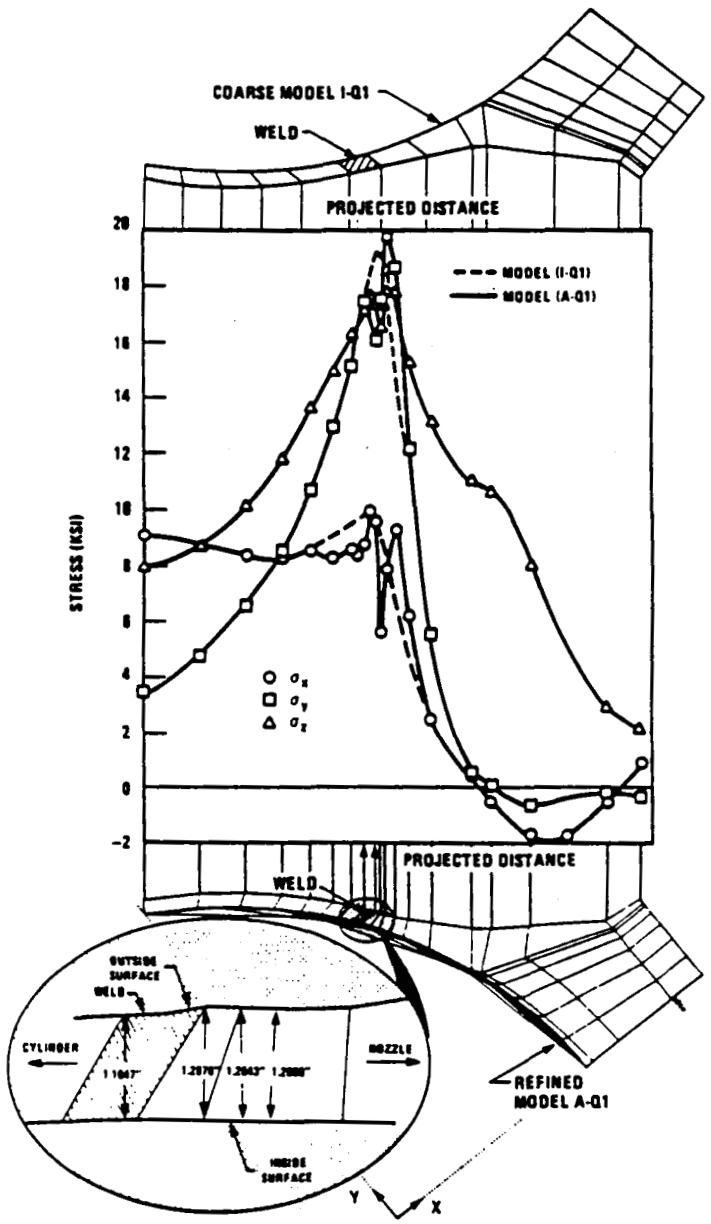

Figure 3. - Suface Mesh Refinement alters Stess Distribution near the Weld Region

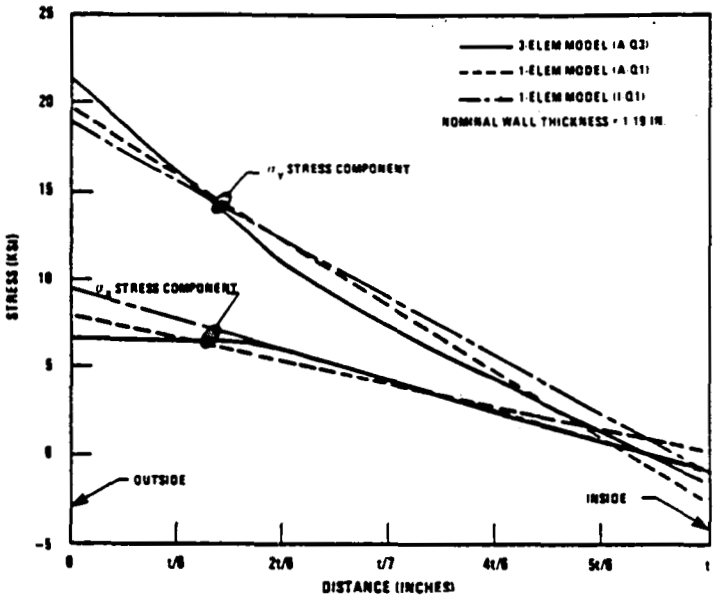

Figure 4. - Mesh Refinement through the thickness has small influence on stresses caused by internal pressure

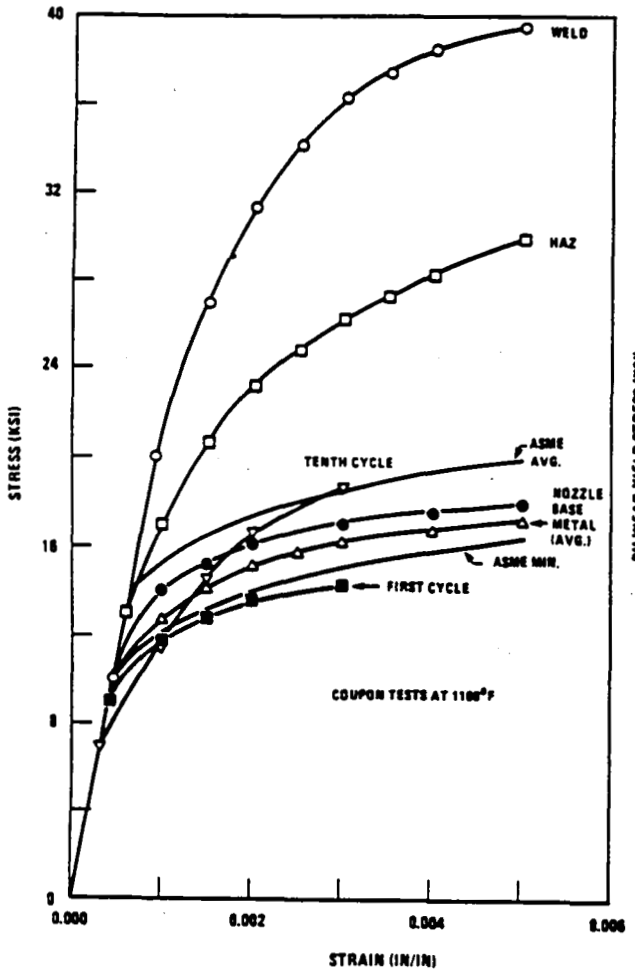

Figure 5. - Material Data obtained from Nozzle Forging

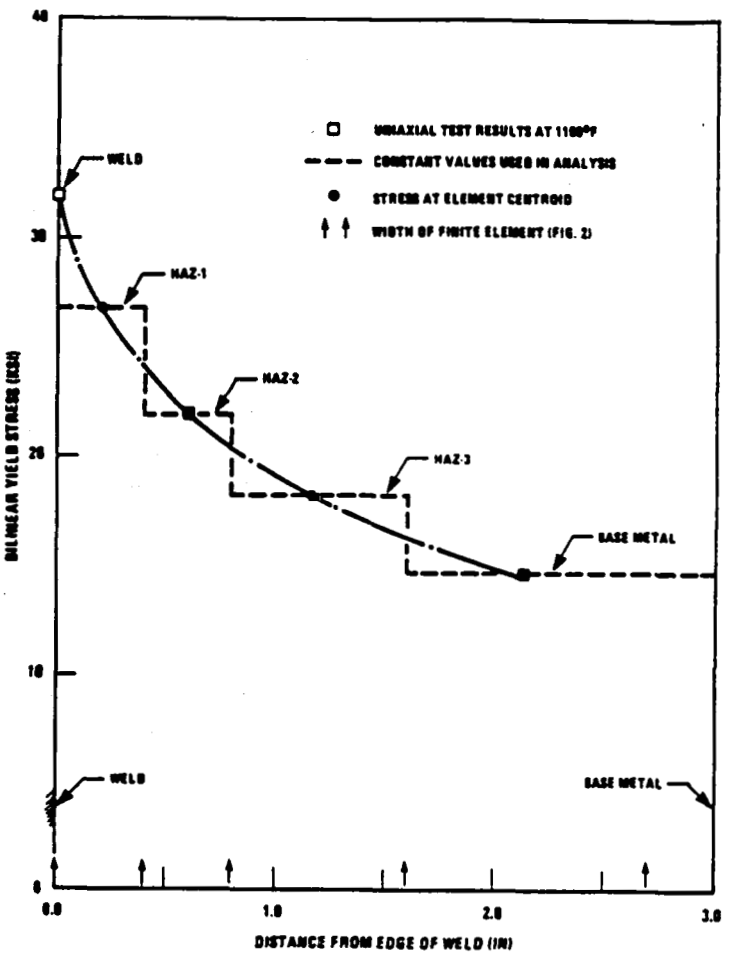

Figure 6. - Yield Stress decreases away from the Weld

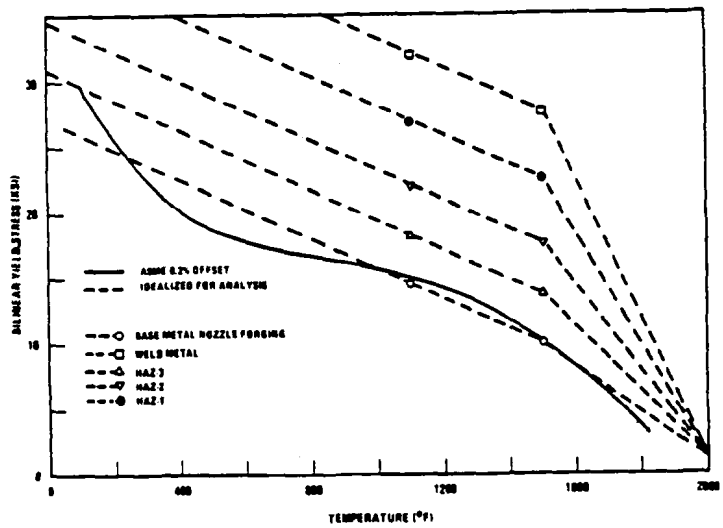

Figure 7. - Temperature Dependence of Yeild Stress, σ_y

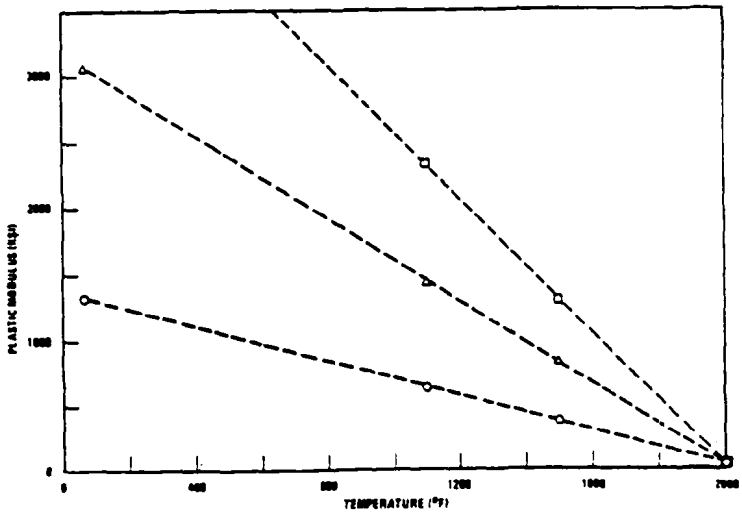

Figure 8. - Temperature Dependence of Plastic Modulus, Σ_p

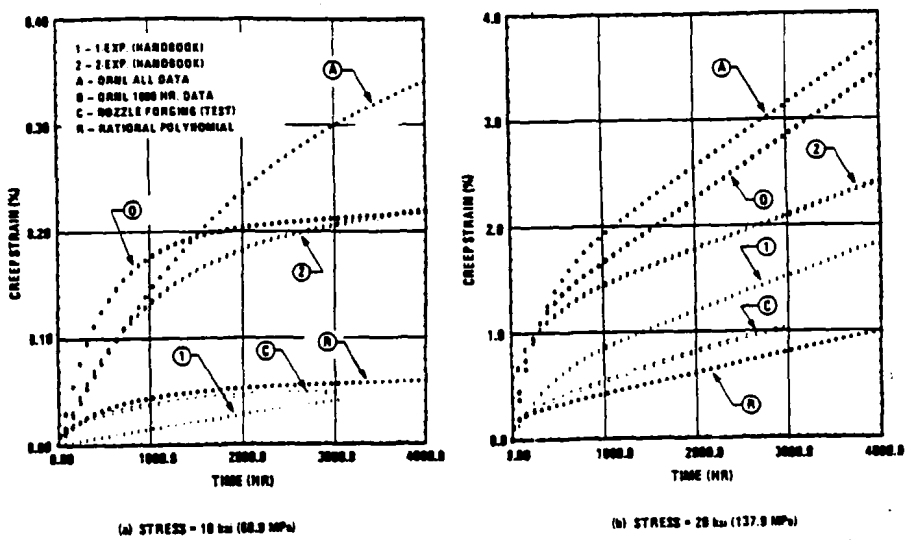

Figure 9. - Comparison of Base Metal Uniaxial Creep Test Data with 304SS Material Representations (593 ^{o}C)

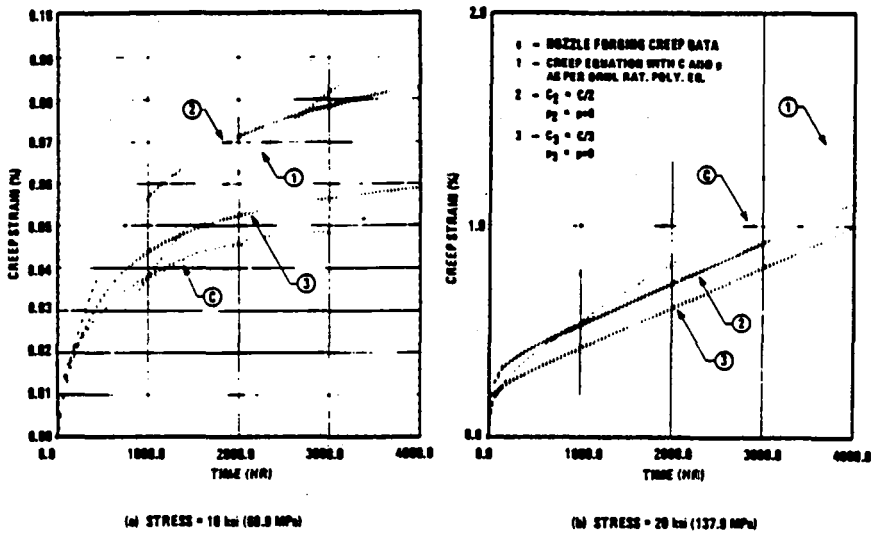

Figure 10. - Rational Polynomial Creep Equation Constants adjusted to fit Base Metal Test Data (593 °C)

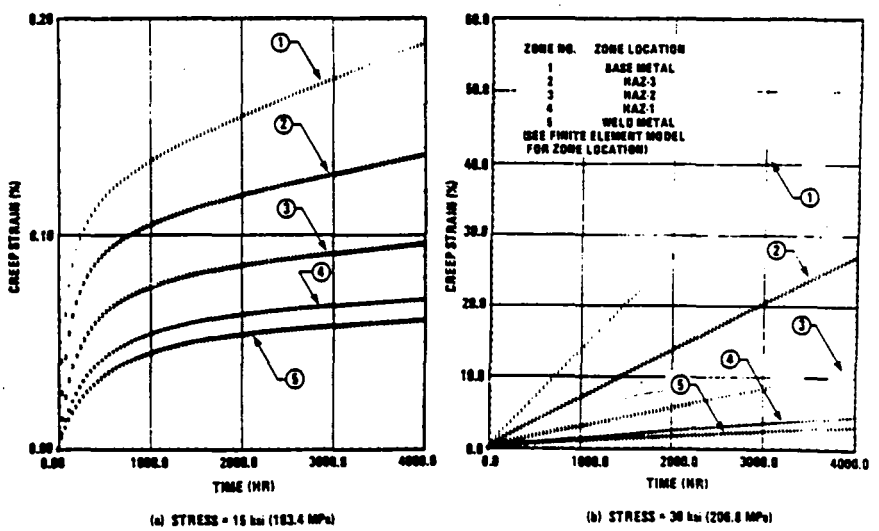

Figure 11. - A 5-Zone Rational Polynomial Creep Representation for Weld Region (593 °C)

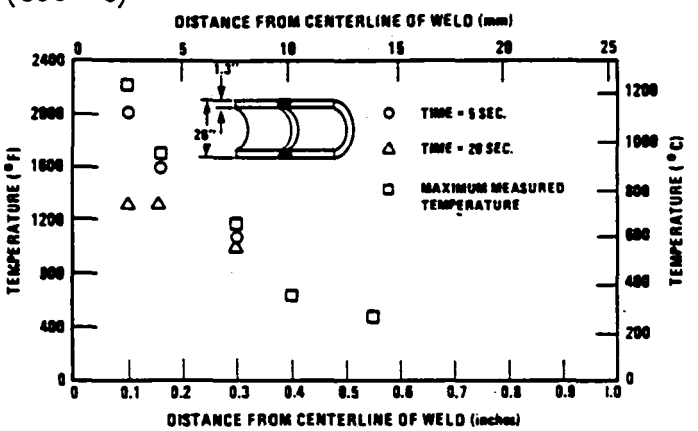

Figure 12. - Temperatures measured during Weld cool-down decrease rapidly with increase in time and distance away from Weld (ref. 10)

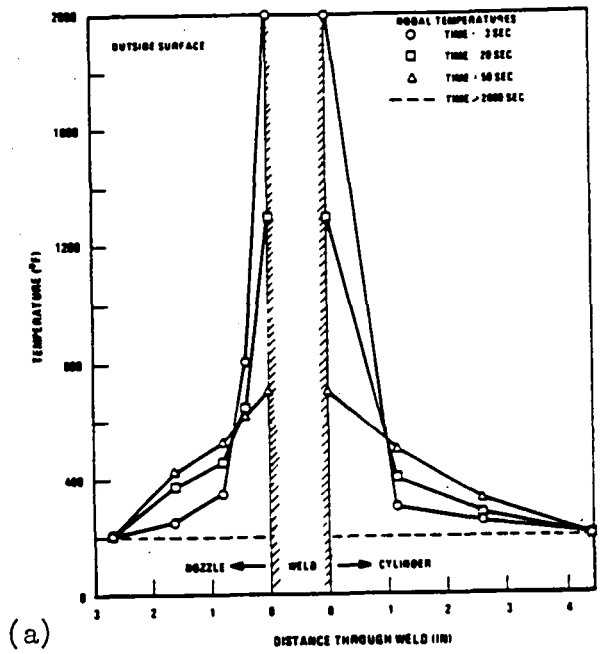

(a)

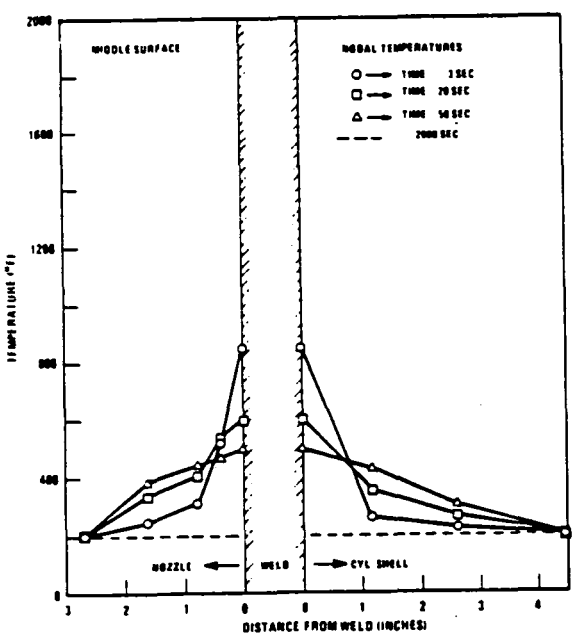

(b)

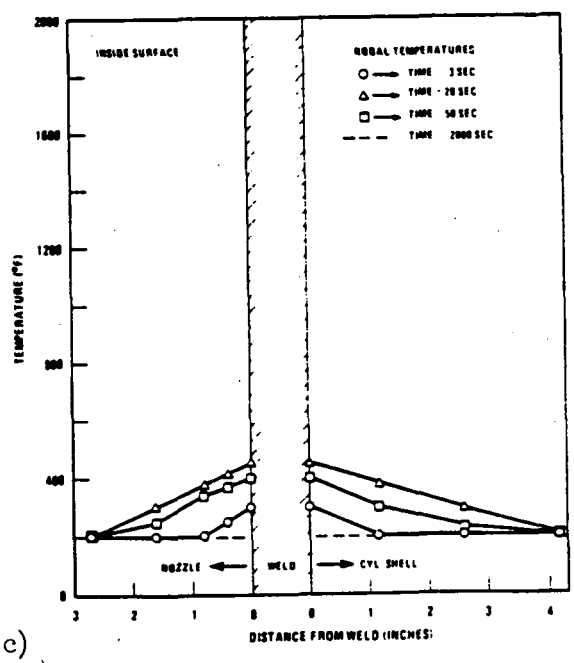

(c)

Figure 13. - Simulation of Weld cool-down temperature distribution

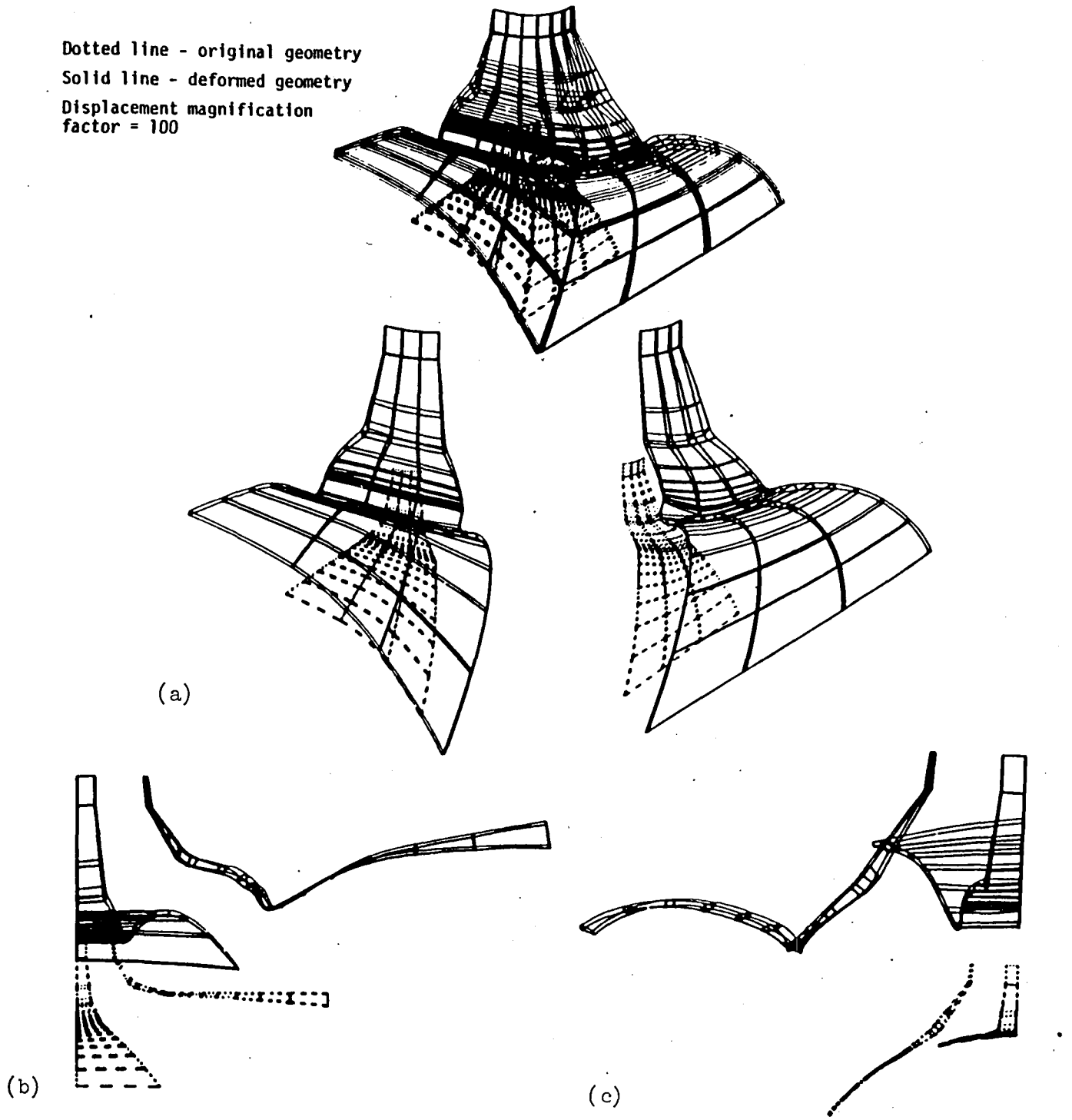

(a) Overall Weld shrinkage deformations

(b) Longitudinal section

(c) Transverse section

Figure 14. - Magnified Nozzle Deformation at the end of Weld cool-down (Includes 156 hours of Creep Hold at zero pressure)

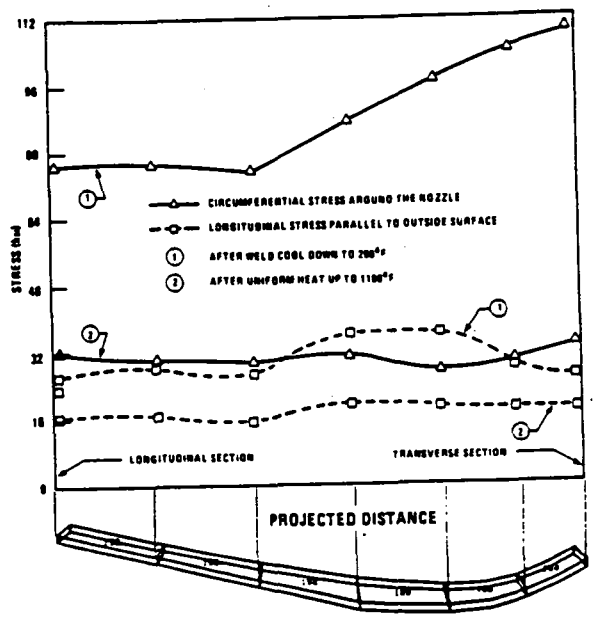

Figure 15. - Weld Residual Stress relaxes around the Circumferential Weld Slice (Nozzle HAZ Outside Surface)

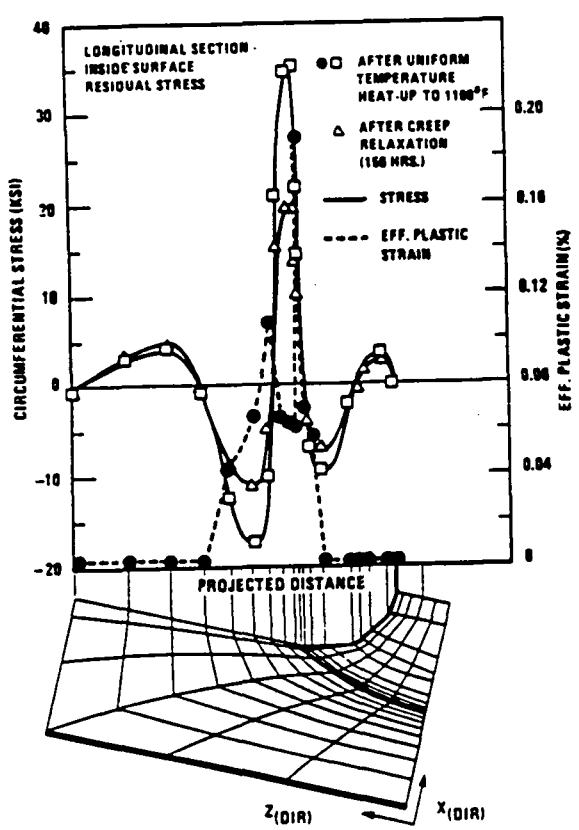

Figure 16. - Weld Residual Stress relaxes significantly during Creep Hold Time

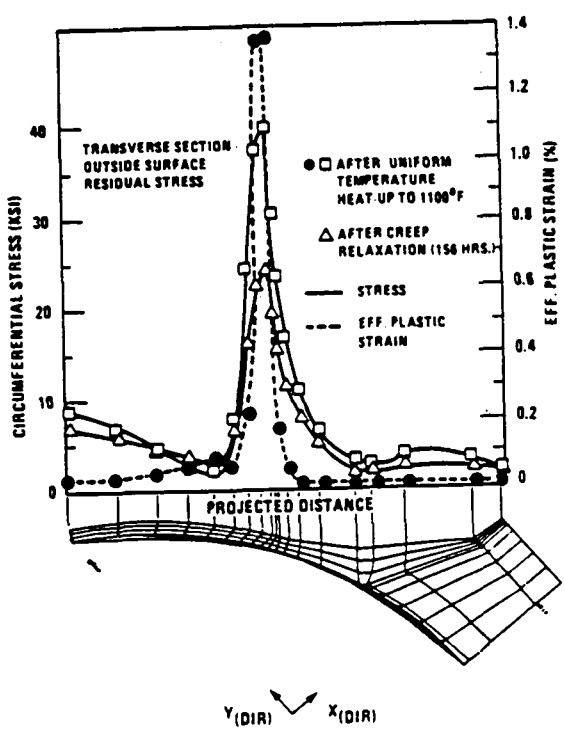

Figure 17. - Weld Residual Stress relaxes significantly during Creep Hold Time